First-principles study of the influences of oxygen defects upon the electronic properties of Nb-doped TiO_2 by GGA + U methods*

Song Chen-Lu(宋晨路), Yang Zhen-Hui(杨振辉), Su Ting(苏 婷), Wang Kang-Kai(王慷慨), Wang Ju(王 菊), Liu Yong(刘 涌)†, and Han Gao-Rong(韩高荣)

State Key Laboratory of Silicon Materials and Department of Materials Science and Engineering, Zhejiang University, Hangzhou 310027, *China*

(Received 22 October 2013; revised manuscript received 15 December 2013; published online 25 March 2014)

The influence of oxygen defects upon the electronic properties of Nb-doped TiO_2 has been studied by using the general gradient approximation (GGA)+U method. Four independent models (i.e., an undoped anatase cell, an anatase cell with a Nb dopant at Ti site (Nb_{Ti}), an anatase cell with a Nb-dopant and an oxygen vacancy (Nb_{Ti}+V_O), and an anatase cell with a Nb-dopant and an interstitial oxygen (Nb_{Ti}+O_i)) were considered. The density of states, effective mass, Bader charge, charge density, and electron localization function were calculated. The results show that in the Nb_{Ti}+V_O cell both e_g and t_{2g} levels of Ti 3d orbits make contributions to the electronic conductivity, and the oxygen vacancies (V_O) collaborate with Nb-dopants to favor the high electrical conductivity by inducing the Nb-dopants to release more excess charges. In Nb_{Ti}+O_i, an unoccupied impurity level appears in the band gap, which served as an acceptor level and suppressed the electronic conductivity. The results qualitatively coincide with experimental results and possibly provide insights into the preparation of TCOs with desirable conductivity.

Keywords: TiO_2, oxygen defects, excess charges, GGA+U method

PACS: 71.15.–m, 71.15.Mb, 81.05.–t **DOI:** 10.1088/1674-1056/23/5/057101

1. Introduction

Recently, the discovery of a new transparent conducting oxide (TCO), anatase Nb:TiO_2 (TNO) films synthetized by the pulsed laser deposition (PLD) technique, has been reported by Furubayashi *et al.*[1] The resistivity of films can reach as low as 2×10^{-4}–3×10^{-4} Ω·cm at room temperature (RT) and the internal transmittance of films is about 90% in the visible light region, showing desirable optoelectronic properties that are comparable to indium tin oxide (ITO). TNO has advantages over ITO, such as high refractive index, high transmittance in the infrared region, and high chemical stability. Additionally, Ti, a major constituent of TNO, is much more abundant in the Earth's crust than In.[2] Therefore, TNO is regarded as one of the most promising candidates for TCO, and this has motivated large amounts of experimental research.[1,3–15] Some consensuses on TNO have been reached; for instance, anatase TNO films exhibit intrinsic transparent metallic behaviors whether it grows on $LaAlO_3$ substrate epitaxially or on glass substrate polycrystallinely.[9,11] Contrarily, rutile Nb:TiO_2 films exhibit insulating behaviors with 2–3 orders higher room temperature electrical resistivity.[14] Kafizas *et al.* also demonstrated that low oxygen pressure (P_{O_2}) favors metallic-like TNO films, whereas higher P_{O_2} hampers the conductivity and results in a n-type semiconductor.[4] Notably, conductive TNO is changed into insulating films with $p > 10^6$ Ω·cm under post-annealing treatment in air.[9]

TNO is a new TCO material and there have been intensive experimental studies of its potential application in electronics, optoelectronics, and photovoltaics, most of which rely on the control of free carrier generation, transport, and recombination. Theoretical studies of the electronic properties in TNO are, therefore, of great importance, but the lack of a correct description has hampered the useful contribution of theory. First-principles calculations in the frame work of density function theory (DFT) using local density approximation (LDA),[16] or general gradient approximation (GGA),[17–20] are known as the standard DFT,[21,22] which means that no corrections have been employed to deal with the strong, localized valence orbits. They usually suffer from the self-interaction error (SIE)[23] and lead to unphysical delocalization of the electronic states. To remedy this problem, two methodologies are widely used: hybrid functionals[24–27] and GGA+U functionals.[28] The GGA+U uses the addition of the Hubbard+U term, which has the effect of dragging the occupation number of a state to either 1 or 0. A close relation between the U and HF terms can be shown mathematically.[29] Thus, the addition of a +U term can also reduce the SIE.[30] The use of hybrid functionals[31,32] is computationally quite intensive and consequently the GGA+U method[33–40] is more widely adopted. In the application of the GGA+U method, the +U parameter is usually prepared using a linear response approach,[41] or by referring the first and second ionization energies (or several excitation energies) of an atom,[42] or by fitting the calculated bandgap to the experimental value.[34]

*Project supported by the National Natural Science Foundation of China (Grant Nos. 51002135 and 51172200) and the Fundamental Research Funds for the Central Universities of Ministry of Education of China (Grant No. 2013QNA4011).

†Corresponding author. E-mail: liuyong.mse@zju.edu.cn

© 2014 Chinese Physical Society and IOP Publishing Ltd

Several theoretical studies have been published for TiO_2 and related materials using this method. By using the GGA+U method, Morgan *et al.* calculated the electronic structures of Nb-doped anatase and rutile TiO_2, finding strongly localized small polarons in Ti sublattice for both phases.[35] Therefore, they proposed that the metallic conduction behaviors in thin-film Nb-doped anatase results from some alternative causes (such as additional defects, sample morphology, and synthesis history) instead of the intrinsic properties of the anatase lattice. However, their analysis failed to reproduce the qualitative differences between the two polymorphs.

Thus, accurate descriptions of the electronic properties of TNO films are still flimsy. As is known, the conductivity in TNO should be relevant to the nonstoichiometry[18,43] of the system. The XPS measurements also demonstrated the coexistence of Ti^{3+} and Nb^{4+} states in TNO films,[5] which implies that oxygen defects in the vicinity of the Nb dopants play an essential role in electronic properties of TNO. In the present study, in order to shed light on the roles of oxygen defects and their interactions with Nb-dopants in anatase TNO, four independent models, including an undoped anatase cell, an anatase cell with a Nb dopant at Ti site cell (Nb_{Ti}), a Nb-dopant and an oxygen vacancy co-doped cell (Nb_{Ti}+V_O), and a Nb-dopant and an interstitial oxygen co-doped cell (Nb_{Ti}+O_i), were studied by using GGA+U. The rest of this article is arranged as follows. The calculation method is described in Section 2. In Section 3, we present the results and a discussion of our calculations, which are related to the electronic properties. The concluding remarks are given in Section 4, along with the summary of the study.

2. Computational details

All of the spin-polarized DFT calculations were performed by using projector augmented wave (PAW) pseudopotentials, as implemented in the Vienna *ab initio* simulation package (VASP).[44,45] The exchange correlation effects were treated within the generalized gradient approximation (GGA) with the Perdew–Burke–Ernzerhof (PBE) function. Our calculations were all based on an anatase supercell with 48 atoms, as a 2×2×1 repetition of the primitive anatase unit cell. The atomic positions of the simulated structures were optimized until all components of the residual forces were converged to 10^{-2} eV/Å (1 Å = 10^{-10} m). The convergence threshold for the self-consistence-field iteration was set at 10^{-4} eV. The wave functions were expanded into a basis set of plane waves, with a kinetic-energy cutoff of 500 eV for all calculations. The Monkhorst–Pack (MP) mesh of 5×5×5 of $\boldsymbol{k}$-points was used to sample the integration in Brillouin zone in the relaxation calculations while an improved mesh of 9×9×9 of $\boldsymbol{k}$-points was used for the electronic calculations. Actually, these parameters were tested to show enough convergence for the energies. The supercell may be rather small, but DFT calculations on larger systems with this basis are not yet possible for us due to the excessive length of the computing time. The concentrations of Nb atoms (Nb/[Nb+Ti]) in the anatase Nb_{Ti} cell and co-doped models are 6.25 at.%, which are comparable to those of the experiments.[1,9–11] In the present GGA+U calculations, the effective U parameter $U_{\text{eff}} = 7.2$ eV has been used to correct the strong Coulomb interaction between 3d electrons localized on Ti in anatase models. The calculated band gap of undoped anatase TiO_2 is 3.20 eV, in good agreement with the experimental values.

3. Results and discussion

3.1. Optimized structure

Figure 1 shows the crystal structures for the optimized models. The undoped and Nb_{Ti} anatase TiO_2 structures can be easily obtained by performing the structural optimization under the symmetry constrains. However, for co-doped models, it is a little more complicated. On the basis of the symmetry analysis, there are 9 and 6 atomic structures for Nb_{Ti}+V_O and Nb_{Ti}+O_i cells, respectively. The total energies of these optimized cells are plotted in Fig. 2 as a function of the distance between Nb_{Ti} and V_O (r(Nb–V_O)) or O_i (r(Nb–O_i)). For Nb_{Ti}+V_O models, the total energies decrease with the increase of r(Nb–V_O), which is caused by the electrostatic repulsion[18] between the V_O and Nb_{Ti}. The lowest total energy of anatase Nb_{Ti}+V_O cell corresponds to the r(Nb–V_O) with a value of 6.2105 Å. For Nb_{Ti}+O_i models, the total energies approximately go up with the r(Nb–O_i), which is caused by the electrostatic attraction between the O_i and Nb_{Ti}, except for the structure with the smallest r(Nb–O_i) whose short Nb–O bonding raises the extra repulsion energy. The lowest total energy of the anatase Nb_{Ti}+O_i cell corresponds to the r(Nb–O_i) with a value of 3.4073 Å. These tendencies are in accordance with the reports of Kamisaka.[18] The total energies of the models are close to each other. We only focus on the interactions between Nb_{Ti} dopant and a V_O/O_i. The Nb_{Ti}+V_O (Nb_{Ti}+O_i) cell with the lowest total energy is referred to as co-doped Nb_{Ti}+V_O (Nb_{Ti}+O_i) cell in our following calculations. Other structures, with a Nb_{Ti} dopant separated from a V_O/O_i in the cell, do not show any novel result based on expectations from the referred cells, either in band structures or in DOS plots.

Table 1 summarizes the final optimized lattice parameters corresponding to various models (see Fig. 1). The crystal structures remain essentially tetragonal for all doped models (Table 1). In optimized Nb_{Ti} cell, the lattice parameters increase slightly in $x(y)$ directions with a value of 0.5% while they shrink in z direction with a value of 0.1% compared with undoped anatase TiO_2. Compared with the undoped anatase TiO_2, the local TiO_6 octahedrons around the substitutional Nb

atom change slightly. For the nearest local TiO_6 octahedrons in x–y plane, the O–Ti–O bonding along z direction increases from 4.0134 Å in the undoped TiO_2 to 4.0328 Å in the Nb_{Ti} cell, and the Ti atoms displace 0.0293 Å along the z direction, making the symmetry of these TiO_6 octahedrons reduce from S_4 to C_{2v}.

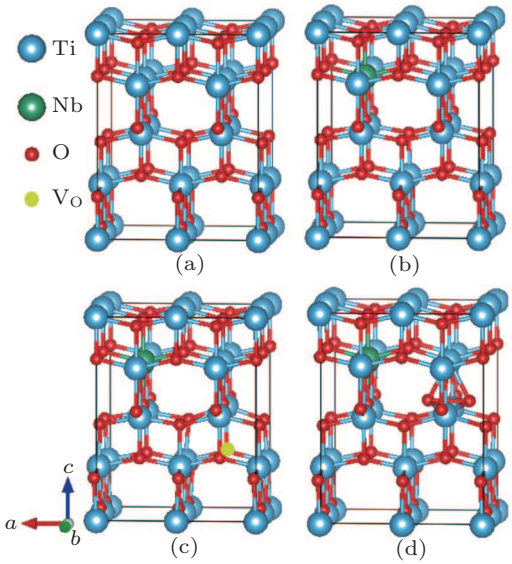


Fig. 1. (color online) The 48-atom 2×2×1 supercell used for anatase (a) undoped TiO_2, (b) Nb_{Ti} cell, (c) Nb_{Ti}+V_O cell, and (d) Nb_{Ti}+O_i cell. The x, y, and z axes are along the crystallographic a, b, and c directions, respectively. Above co-doped structures ((c) and (d)) refer to the models with the lowest total energies in our following calculations.

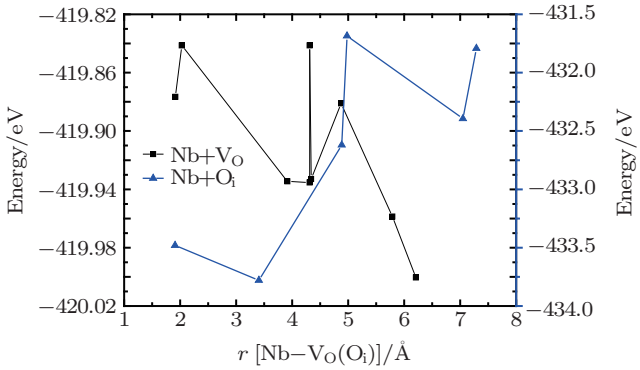


Fig. 2. (color online) Total energies in the anatase optimized Nb_{Ti}+V_O cells (black solid square) and optimized Nb_{Ti}+O_i cells (blue solid triangle) as functions of r(Nb–V_O) and r(Nb–O_i) distances, respectively.

Table 1. Optimized lattice constants, and lattice constants taken from Ref. [18], respectively.

		Undoped	Nb_{Ti}	Nb_{Ti}+V_O	Nb_{Ti}+O_i
a/Å	Cal.	7.6141	7.6544	7.6478	7.6246
	Ref.	7.6331	7.6725	7.6409	7.6374
b/Å	Cal.	7.6141	7.6544	7.6513	7.6021
	Ref.	7.6331	7.6741	7.6529	7.6027
c/Å	Cal.	9.7166	9.7057	9.7213	9.8261
	Ref.	9.7151	9.6957	9.7335	9.8342

In the Nb_{Ti}+V_O cell, the lattice parameters in $x(y)$ directions remain almost unchanged while they increase 0.2% along z direction compared with the Nb_{Ti} cell. The three nearest Ti ions around the V_O displace by 0.0726 Å–0.1362 Å outward from the vacancy site and oppositely the neighboring O ions shift inward by 0.0193 Å–0.1119 Å.

In the Nb_{Ti}+O_i cell, the O_i is settled in a cage-like interstitial space among TiO_6 octahedrons, and close to one lattice oxygen atom. Compared with the Nb_{Ti} cell, the lattice parameters shrink by 0.4% and 0.7% in x and y directions, respectively, while they increase by 1.2% in z direction. The adjacent lattice O anion shifts outward by 0.9196 Å from its original position. The internuclear distance between them (the interstitial oxygen and the adjacent lattice oxygen atom) is 1.9269 Å, compared with that of O_2 gas molecule, that is $r(O–O)_{O_2}$ = 1.21 Å,[18] forming an O–O pair[46], as shown in Fig. 1(d).

3.2. TDOS and PDOS

3.2.1. Anatase Nb_{Ti} Cell

The calculated TDOS and PDOS of the anatase Nb_{Ti} cell using GGA+U are depicted in Fig. 3. Compared with the undoped TiO_2, the remarkable feature in the energy band of the Nb_{Ti} cell is that the band-tail state appears in the CBM (conduction band minimum), mainly consisting of the Ti 3d_{xy} orbits,[3] a t_{2g} levels. The band-tail state is largely contributed by the aforementioned nearest Ti atoms around Nb in the x–y plane (see Figs. A1 and A4). As shown in Figs. 3(b) and 3(c), the energy levels of the Ti 3d orbits are close to those of the Nb 4d orbits, which may lead to a strong hybridization. One can expect that one more electron released by the Nb dopant occupies the Ti 3d_{xy} orbits, inducing the Ti 3d_{xy} energy levels to drop as the continuous band-tail state appearing in the CBM and simultaneously triggering Fermi energy to shift up into the conduction band edge. These behaviors cause a degenerated semi-conductive band structure, showing a typical metallic characteristic.

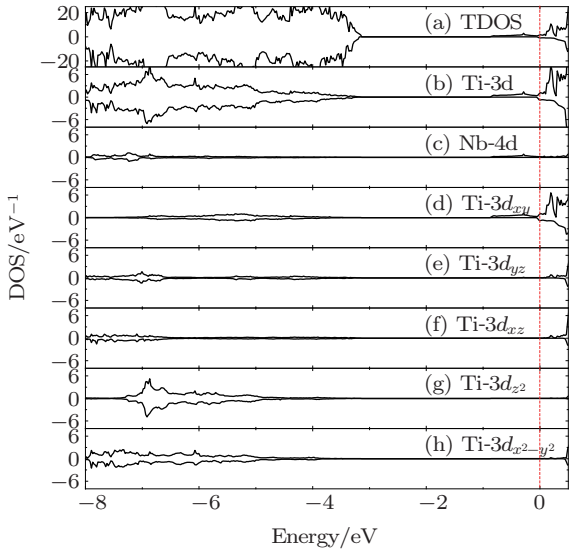


Fig. 3. (color online) The TDOS (a), PDOS (b)–(c) of anatase Nb_{Ti} cell, and PDOS (d)–(h) for Ti atoms in anatase Nb_{Ti} cell. The red dotted line indicates the Fermi level at 0 eV.

3.2.2. Anatase Nb_{Ti}+V_O cell

The DOS and PDOS of Nb_{Ti}+V_O cell are plotted in the Fig. 4. Compared with the Nb_{Ti} cell, the biggest differences are the appearances of an occupied state in the band gap about 1.43 eV beneath the Fermi energy and band-tail states below the CBM, as shown in Fig. 4(a). This midgap level mainly consists of $3d_{xy}$ and $3d_{xz}$ of three Ti atoms surrounding the V_O (Figs. A2 and A5). An impurity state contributed by O 2p orbits appears in the maximum of valence band (VBM), implying an enhancement of coupling between Ti 3d (or Nb 3d) and O 2p in Nb_{Ti}+V_O cell. Notably, the band-tail states are mainly contributed by the Ti $3d_z^2$ and $3d_{x^2-y^2}$ orbits, e_g levels, instead of t_{2g} level. This is due to more excess electrons being provided by the oxygen vacancy occupying the 3d orbits of nearest Ti ions, which make the Fermi level shift into a higher energy. Furthermore, a very narrow gap with a width of about 0.07 eV can be found in the vicinity of the Fermi level, separating the occupied Ti e_g orbits and unoccupied t_{2g} orbits. This gap is so narrow that electrons can be easily transferred over it by very small thermal excitation. Therefore, both t_{2g} and e_g levels of Ti 3d orbits contribute to the electronic conductivity in the Nb_{Ti}+V_O cell.

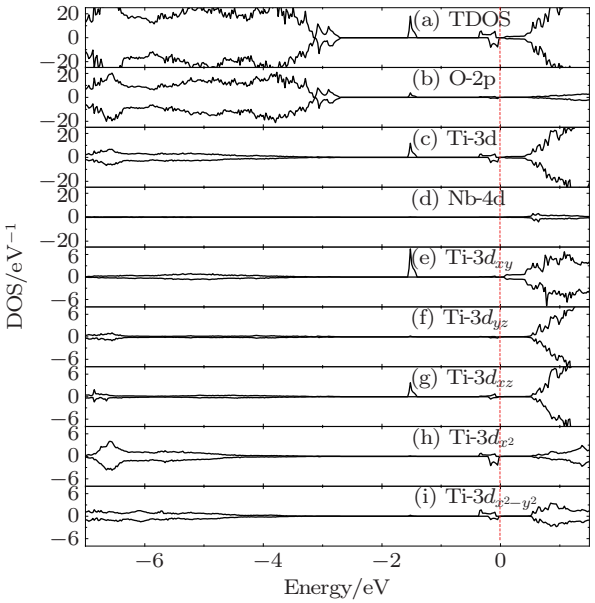


Fig. 4. (color online) The TDOS (a), PDOS (b)–(c) of anatase Nb_{Ti}+V_O cell, and PDOS (e)–(i) for Ti in anatase Nb_{Ti}+V_O cell. The red dotted line indicates the Fermi level at 0 eV.

3.2.3. Anatase Nb_{Ti}+O_i cell

One can find that the DOS of the Nb_{Ti}+O_i cell is quite different from those of the Nb_{Ti} cell, with two pronounced peaks appearing in the band gap while the band-tail states disappear in the band gap, as shown in Fig. 5. The midgap states are spin-polarized, splitting into one occupied state and one unoccupied state. These two midgap levels are situated about 0.60 eV and 2.04 eV above the VBM, as shown in Fig. 5(a), and have certainly contributed by O $2p_x$ to the aforementioned O–O pair (Figs. A3 and A6). This can be understood as the O_i atom introducing two unpaired 2p electrons in the Nb_{Ti}+O_i cell and capturing the extra electrons emitted by the Nb atom, leading to the emergence of an occupied impurity level and the disappearance of the band-tail state. Additionally, the unoccupied O 2p levels are situated at the band gap; thus, the interstitial oxygen suppresses the electronic conductivity.

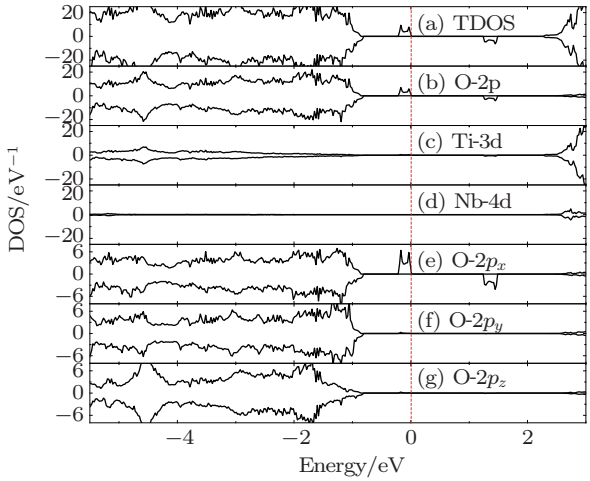


Fig. 5. (color online) The TDOS (a), PDOS (b)–(d) of anatase Nb_{Ti}+O_i cell, and PDOS (e)–(f) for O atoms in anatase Nb_{Ti}+O_i cell. The red dotted line indicates the Fermi level at 0 eV.

3.3. Effective mass and Bader charge analysis

From the band structure, the effective mass of the carriers at the CBM can be deduced by using the following equation[17]

$$\frac{1}{m_n^*} = \frac{1}{\hbar^2}\frac{\mathrm{d}^2E(k)}{\mathrm{d}k^2}, \tag{1}$$

where m_n^* is the effective mass, h is the reduced Planck constant, and $E(k)$ is the eigenvalue of the Hamiltonian operator at k. The conduction band in the vicinity of the extrema is assumed to be parabolic; hence, the effective mass will be constant in these areas. The values of the calculated m_n^* are shown in Table 2. Apparently, the m_n^* for the present models are all anisotropic, where the m_n^* along the c-axis is about 6–50 times larger than the values along the $a(b)$-axis. The results of pure anatase TiO_2 and anatase Nb_{Ti} cell are consistent with the experimental results that m_n^* along the a- and c-axis are $\sim 0.6m_0$ and $\sim 3.3m_0$, respectively, where m_0 is the free electron mass.[13] For the anatase Nb_{Ti}+O_i co-doped model, the effective masses are slightly larger than those of the Nb_{Ti} cell or Nb_{Ti}+V_O cell, especially in the c-axis. These results show that the incorporation of interstitial oxygen to the Nb_{Ti} cell increases electronic effective mass, deteriorating to the electronic mobility. These results also imply that epitaxial growth along [001] direction possibly leads into the smaller sheet resistance due to the smaller m_n^* in $a(b)$ directions.

Table 2. The effective mass for various anatase models (m_0 is the free electron mass).

	Undoped	Nb_{Ti}	Nb_{Ti}+V_O	Nb_{Ti}+O_i
m^*_{xx}/m_0	0.60	0.66	0.64	0.73
m^*_{yy}/m_0	0.60	0.66	0.75	0.78
m^*_{zz}/m_0	3.85	6.66	24.23	41.96

To further quantitatively investigate charge transfers, the charges of Ti, Nb, and O in various models were calculated using Bader charge analysis.[47,48] The atomic charges of Ti and O in undoped TiO_2 are about $+2.43e$, $-1.22e$, respectively. Both values deviate from the nominal values expected in a purely ionic state (Ti: $+4e$; O: $-2e$). This deviation partially reflects the covalent character of the bonds between Ti and O. In the Nb_{Ti} cell the charge of substitutional Nb atom is $+2.74e$, which is $0.31e$ larger than those of Ti atoms, indicating that extra electrons are released by the doping atom (Nb).

In the Nb_{Ti}+V_O cell, the charge of Nb atom is $+2.83e$, reflecting that the introduction of oxygen vacancy makes Nb release more free electrons than those of the Nb_{Ti} cell. We can also find that the average charges of three nearest Ti ions around the oxygen vacancy substantially decrease from the average bulk value of $+2.41e$ in Nb_{Ti} cell to $+2.12e$. The average charges of nearest O ions in x–z plane increase about $0.07e$. These results indicate that the two excess electrons corresponding to the neutral vacancy are mainly distributed among the Ti ions nearby the vacancy site, and hence should occupy certain electronic states of those ions. Indeed, this can be seen clearly from the (P)DOS as discussed in the aforementioned section.

In the Nb_{Ti}+O_i cell, the charge of O_i–O pair is $-1.83e$ which is lower than that of O ions in undoped TiO_2 or Nb_{Ti} cell. Therefore, the O_i–O pair can capture the electrons belong to its nearby ions, exhibiting the character of acceptor. Exactly, as shown in the Fig. 5, the O 2p states separated by Fermi energy appear in the band gap.

3.4. Contour plots of charge density and electron localization function (ELF)

The contour plots of charge density for the anatase Nb_{Ti}, Nb_{Ti}+V_O cell, and Nb_{Ti}+O_i cell have been calculated as shown in Fig. 6. As displayed in Fig. 6(b), there are a certain amount of electrons distributed around the oxygen vacancy. From Fig. 6(d) it can be seen that the bonding effects can be found between O_i and its nearby Ti ions in the Nb_{Ti}+O_i model. The electron localization functions (ELF) for these models were also calculated as shown in Fig. 7. The ELF is a scalar continuous function bounded between 0 and 1, a value of 1 indicates that electrons are fully localized and a value of 0 implies that the electrons are fully delocalized or that there is no electron in that place. Therefore, a value between 0 and 1 indicates the probability of the formation of an electron-gas-like pair.[49] Combined with the results of Figs. 6 and 7, delocalized electrons around oxygen vacancy and localized electrons around interstitial oxygen can be found. The aforementioned analysis of electron density

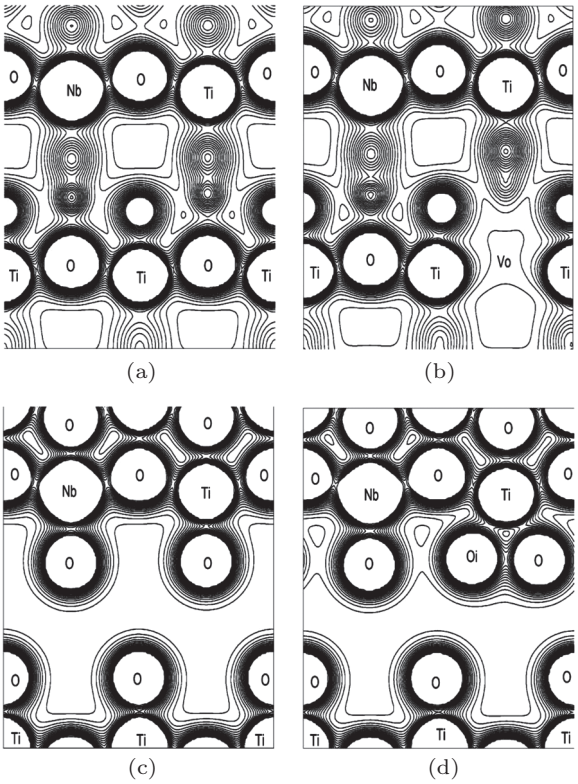


Fig. 6. Panels (a) and (c) are the contour charge density for anatase Nb_{Ti} cell. Panel (b) is the contour plot of Nb_{Ti}+V_O cell for crystal plane corresponding to panel (a). Panel (d) is the contour charge density for crystal plane of anatase Nb_{Ti}+O_i cell corresponding to panel (c). The dark and light regions indicate the increasing and decreasing charge densities, respectively (contour line interval is 0.05 e/Å^3).

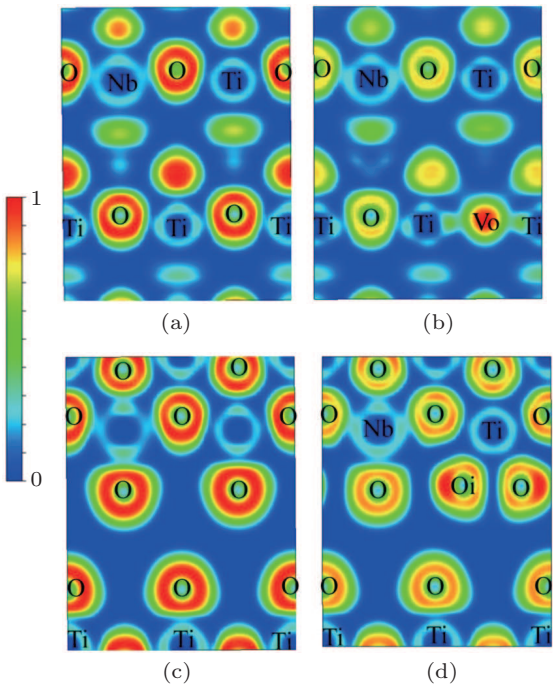


Fig. 7. (color online) Panels (a)–(d) are the electron localization function (ELF) contour plots corresponding to the Figs. 6(a)–6(d), respectively. The red indicates 1 and blue refers to 0.

and ELF show that the excess electrons released by V_O can distribute to the nearby ions while O_i behaves as an acceptor to capture electrons in corresponding co-doped anatase models, which is consistent with the calculated results of T(P)DOS and Bader charge analysis.

4. Conclusions

Four independent anatase models (namely, undoped cell, Nb_{Ti} cell, Nb_{Ti}+V_O cell, and Nb_{Ti}+O_i cell) were investigated by means of the GGA+*U* method. The calculated results show that the anatase Nb_{Ti} cells are degenerated semiconductors with a typical n-type degenerated characteristic in their electronic structure, which is in good agreement with the experimental results that anatase Nb:TiO_2 film is an intrinsic transparent metal.

In the Nb_{Ti}+V_O co-doped supercell, more excess electrons provided by the oxygen vacancy occupy the 3d orbits of Ti atoms nearby the V_O, leading to the formation of occupied midgap levels and band-tail states. The results of Bader charge analysis also show that the introduction of oxygen vacancy can make Nb release more free electrons than the Nb_{Ti} cell, showing that V_O can collaborate with Nb-dopants to favor high conductivity.

For the Nb_{Ti}+O_i co-doped model, two spin-polarized impurity states are located in the band gap, splitting into one occupied state and one unoccupied state. The unoccupied impurity level can behave as an acceptor level to capture free electrons, which is in agreement with the results of Bader charge analysis, charge density, and ELF. In addition, the calculated results also show that the effective mass of the anatase Nb_{Ti}+O_i co-doped model is larger than those of the Nb_{Ti} cell or Nb_{Ti}+V_O cell. Thus, one can expect that the introduction of O_i to the Nb_{Ti} cell deteriorates the excellent conductivity of TNO films, especially for O-rich growth conditions that favor the incorporation of interstitial oxygen in the anatase Nb_{Ti} cell.

Appendix A

Figures A1, A2, and A3 are PDOS plots calculated for each atom in the Nb_{Ti} cell, Nb_{Ti}+V_O cell, and Nb_{Ti}+O_i cell, respectively. The red dotted line indicates the Fermi level at 0 eV, and the corresponding 48-atom 2×2×1 supercells of Nb_{Ti} cell, Nb_{Ti}+V_O cell, and Nb_{Ti}+O_i cell are presented in Figs. A4, A5, and A6, respectively. The *x*, *y*, and *z* axes are along the crystallographic *a*, *b*, and *c* directions, respectively. The marked atoms in the supercells refer to those numbered in PDOS.

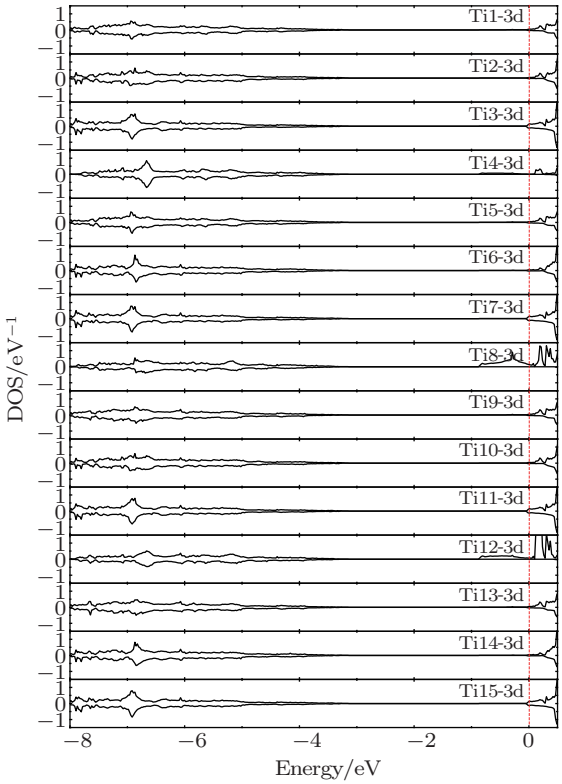


Fig. A1. (color online) PDOS plots calculated for 3d orbits of each Ti atom in Nb_{Ti} cell.

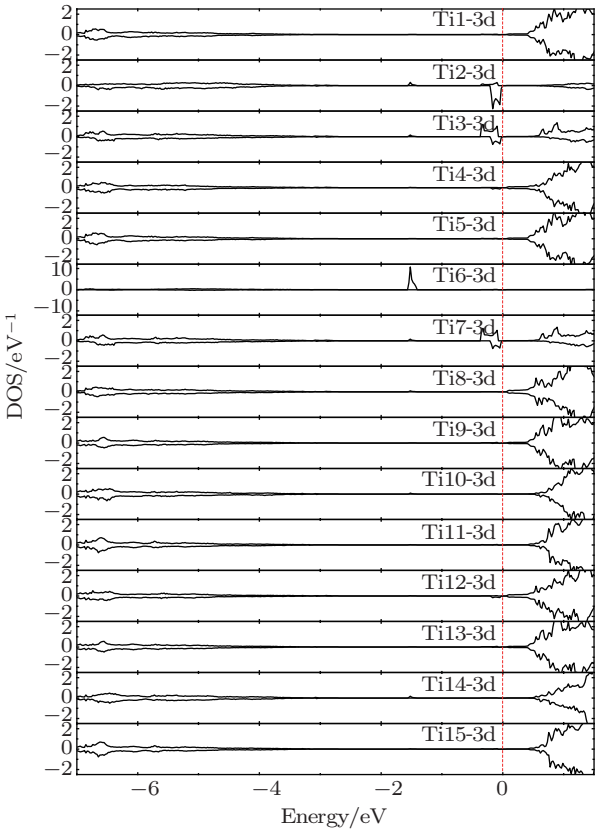


Fig. A2. (color online) PDOS plots calculated for 3d orbits of each Ti atom in Nb_{Ti}+V_O cell.

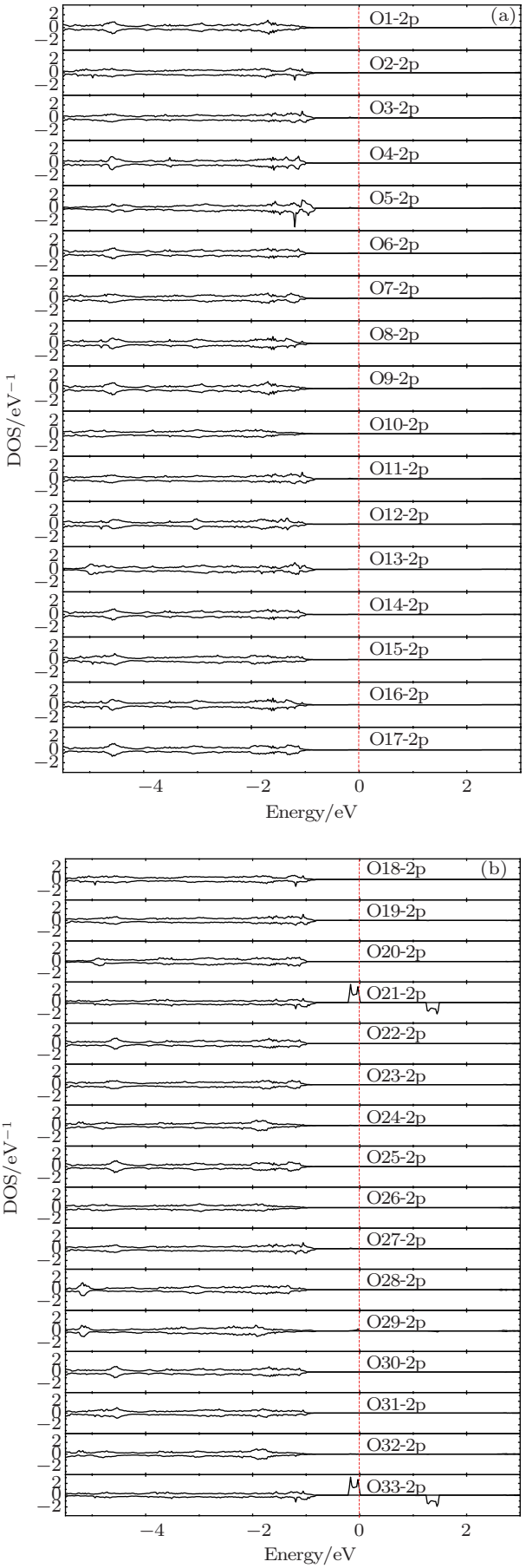


Fig. A3. (color online) PDOS plots calculated for 2p orbits of each O atom in Nb_{Ti}+O_i cell. (a) From O1-2p to O17-2p. (b) From O18-2p to O33-2p.

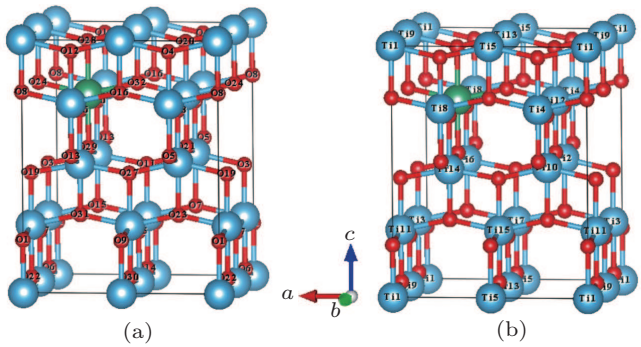


Fig. A4. (color online) 48-atom 2×2×1 supercell used for anatase Nb_{Ti} cell. The marked atoms correspond to those in Fig. A1. (a) O atoms; (b) Ti atoms.

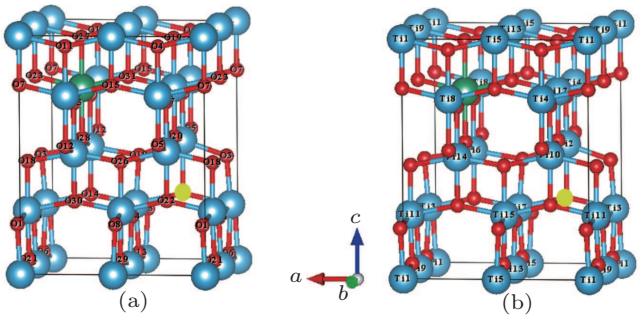


Fig. A5. (color online) 48-atom 2×2×1 supercell used for anatase Nb_{Ti}+V_O cell. The marked atoms correspond to those in Fig. A2. (a) O atoms; (b) Ti atoms.

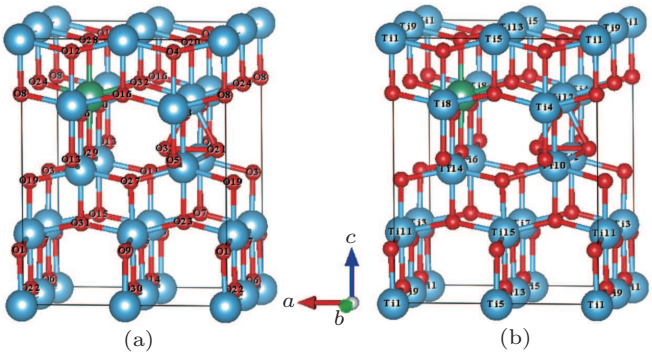


Fig. A6. (color online) 48-atom 2×2×1 supercell used for anatase Nb_{Ti}+O_i cell. The marked atoms correspond to those in Fig. A3. (a) O atoms; (b) Ti atoms.

References

[1] Furubayashi Y, Hitosugi T, Yamamoto Y, Inaba K, Kinoda G, Hirose Y, Shimada T and Hasegawa T 2005 *Appl. Phys. Lett.* **86** 252101

[2] Hitosugi T, Yamada N, Nakao S, Hirose Y and Hasegawa T 2010 *Phys. Status Solidi* **207** 1529

[3] Mulmi D D, Sekiya T, Kamiya N, Kurita S, Murakami Y and Kodaira T 2004 *J. Phys. Chem. Solids* **65** 1181

[4] Kafizas A, Dunnill C W and Parkin I P 2010 *J. Mater. Chem.* **20** 8336

[5] Yang J Y, Han Y L, He L, Dou R F, Xiong C M and Nie J C 2012 *Appl. Phys. Lett.* **100** 202409

[6] Yamada N, Hitosugi T, Kasai J, Hoang N L H, Nakao S, Hirose Y, Shimada T and Hasegawa T 2009 *J. Appl. Phys.* **105** 123702

[7] Sheppard L, Bak T, Nowotny J, Sorrell C C, Kumar S, Gerson A R, Barnes M C and Ball C 2006 *Thin Solid Films* **510** 119

[8] Zhang S, Ogale S B, Yu W, Gao X, Liu T, Ghosh S, Das G P, Wee A T S, Greene R L and Venkatesan T 2009 *Adv. Mater.* **21** 2282

[9] Hitosugi T, Ueda A, Nakao S, Yamada N, Furubayashi Y, Hirose Y, Shimada T and Hasegawa T 2007 *Appl. Phys. Lett.* **90** 212106

[10] Zhao L, Zhao X, Liu J, Zhang A, Wang D and Wei B 2010 *J. Sol–Gel Sci. Technol.* **53** 475
[11] Yang J Y, Li W S, Li H, Sun Y, Dou R F, Xiong C M, He L and Nie J C 2009 *Appl. Phys. Lett.* **95** 213105
[12] Liu J, Zhao X, Duan L, Cao M, Sun H, Shao J, Chen S, Xie H, Chang X and Chen C 2011 *Appl. Surf. Sci.* **257** 10156
[13] Hirose Y, Yamada N, Nakao S, Hitosugi T, Shimada T and Hasegawa T 2009 *Phys. Rev. B* **79** 165108
[14] Zhang S X, Kundaliya D C, Yu W, Dhar S, Young S Y, Salamanca-Riba L G, Ogale S B, Vispute R D and Venkatesan T 2007 *J. Appl. Phys.* **102** 013701
[15] Gillispie M A, van Hest M F A M, Dabney M S, Perkins J D and Ginley D S 2007 *J. Appl. Phys.* **101** 033125
[16] Liu X D, Jiang E Y, Li Z Q and Song Q G 2008 *Appl. Phys. Lett.* **92** 252104
[17] Zhang R S, Liu Y, Gao Q, Teng F, Song C L, Wang W and Han G R 2011 *J. Alloys Compd.* **509** 9178
[18] Kamisaka H, Hitosugi T, Suenaga T, Hasegawa T and Yamashita K 2009 *J. Chem. Phys.* **131** 034702
[19] Hitosugi T, Kamisaka H, Yamashita K, Nogawa H, Furubayashi Y, Nakao S, Yamada N, Chikamatsu A, Kumigashira H, Oshima M, Hirose Y, Shimada T and Hasegawa T 2008 *Appl. Phys. Express* **1** 111203
[20] Zhang R S, Liu Y, Teng F, Song C L and Han G R 2012 *Acta Phys. Sin.* **61** 017101 (in Chinese)
[21] Hohenberg P 1964 *Phys. Rev.* **136** B864
[22] Kohn W and Sham L J 1965 *Phys. Rev.* **140** A1133
[23] Perdew J P 1981 *Phys. Rev. B* **23** 5048
[24] Heyd J, Scuseria G E and Ernzerhof M 2003 *J. Chem. Phys.* **118** 8207
[25] Batista E, Heyd J, Hennig R, Uberuaga B, Martin R, Scuseria G, Umrigar C and Wilkins J 2006 *Phys. Rev. B* **74** 121102
[26] Becke A D 1993 *J. Chem. Phys.* **98** 5648
[27] Lee C, Yang W and Parr R G 1988 *Phys. Rev. B* **37** 785
[28] Anisimov V I, Zaanen J and Andersen O K 1991 *Phys. Rev. B* **44** 943
[29] H H 2004 *Kotai Butsuri* **39** 743
[30] Tsuda N N K, Fujimori A and Siratori K 1993 *Electronic Conduction in Oxides* (2nd edn.) (Shokabo Tokyo)
[31] Lee H Y and Robertson J 2013 *J. Appl. Phys.* **113** 213706
[32] Janotti A, Varley J B, Rinke P, Umezawa N, Kresse G and van de Walle C G 2010 *Phys. Rev. B* **81** 085212
[33] Kamisaka H, Mizuguchi N and Yamashita K 2012 *J. Mater. Sci.* **47** 7522
[34] Yang K, Dai Y and Huang B 2009 *Chemphyschem.* **10** 2327
[35] Morgan B J, Scanlon D O and Watson G W 2009 *J. Mater. Chem.* **19** 5175
[36] Zhou T G, Liu Z Q and Zuo X 2012 *Chin. Phys. Lett.* **29** 047503
[37] Zahid A, Iftikhar A, Banaras K and Imad K 2013 *Chin. Phys. Lett.* **30** 047504
[38] Xu G G, Wu J, Chen Z G, Lin Y B and Huang Z G 2012 *Chin. Phys. B* **21** 097401
[39] Guo Y, Ai J J, Gao T and Ao B Y 2013 *Chin. Phys. B* **22** 057103
[40] Zhang W and Tong P Q 2013 *Chin. Phys. B* **22** 066201
[41] Cococcioni M and de Gironcoli S 2005 *Phys. Rev. B* **71** 035105
[42] Janotti A, Segev D and van de Walle C 2006 *Phys. Rev. B* **74** 045202
[43] Na-Phattalung S, Smith M, Kim K, Du M H, Wei S H, Zhang S and Limpijumnong S 2006 *Phys. Rev. B* **73** 125205
[44] Kresse G and Hafner J 1994 *Phys. Rev. B* **49** 14251
[45] Kresse G and Furthmüllerb J 1996 *Comput. Mater. Sci.* **6** 15
[46] Peng H 2008 *Phys. Lett. A* **372** 1527
[47] Henkelman G, Arnaldsson A and Jónsson H 2006 *Comput. Mater. Sci.* **36** 354
[48] Sanville E, Kenny S D, Smith R and Henkelman G 2007 *J. Comput. Chem.* **28** 899
[49] Becke A D and Edgecombe K E 1990 *J. Chem. Phys.* **92** 5397